
Article:
Ma, H-J, Zhao, H-X, Wang, L et al. (2 more authors) (2017) Modeling and investigation of a steam-water injector. Energy Conversion and Management, 151. pp. 170-178. ISSN 0196-8904

https://doi.org/10.1016/j.enconman.2017.08.068

Modeling and investigation of a steam-water injector

Huijun Ma[1], Hongxia Zhao*[1], Lei Wang[2], Zeting Yu[1], Xiaoan Mao[3]

[1]School of Energy and Power Engineering, Shandong University, Jinan 250061, P. R. China

[2]School of Control Science and Engineering, Shandong University, Jinan 250061, P. R. China.

[3]Faculty of Engineering, University of Leeds, Leeds LS2 9JT, United Kingdom

Abstract

A one-dimensional mathematical model of the steam-water two-phase injector is presented. This model offers a method of estimating critical conditions of steam at the site of the motive nozzle throat, based on the local sound velocity in that area. Fluid thermal properties were based on a real fluid approach, where the CoolProp database was used. A different method was adopted to formulate governing equations for all passages of the injector based on the principles of the conservation of mass, momentum, and energy. The pressure profiles of the injector at different inlet steam pressure and inlet water pressure were used to validate the proposed model; they agreed well, with a maximum relative rate of error within 9.5％. Based on the validated model, the influence of different area ratios and coefficients of the diverse sections on the performance of an injector used in district heating was investigated. The main inlet parameters - steam pressure and water pressure - were within the range of 0.20–0.60 MPa and 0.14–0.49 MPa. The exergy destruction rate for every steam-water injector

component was also computed. The results illustrated that the injector discharge pressure increases with the throat area ratio of the motive nozzle and mixing chamber. The isentropic efficiency coefficients of the converging section and diverging section of motive nozzle affects the entrainment ratio and compression ratio differently. The main irreversibility occurs in steam nozzle (41.34%) and mixing chamber (57.95%). The exergy efficiency of the injector decreases with the increase of mass entrainment ratio. It also increases in coordination with the increase of inlet steam pressures, and decreases with the increase of inlet water pressures.

1. Introduction

Injector and ejector, are important devices used in many industrial applications, because they are simple, without moving parts and do not need an external energy supply system **[1,2]**. Generally, recovering energy and boosting pressure are the main purposes of their application. For an ejector, usually both the primary flow and secondary flow are steam or vapor. For an injector, the primary flow is usually steam or vapor, while the secondary flow is liquid. The injector is also referred to as the jet pump in many applications. Furthermore, there exists a profound difference between the ejector and injector. For example, the entrainment ratio of the ejector is generally less than 1 **[1,3]**, while the entrainment ratio for the injector is much greater than 1 **[4]**. Moreover, the exit pressure of an ejector is lower than the primary flow pressure **[1]**, while the exit pressure of an injector can be higher than the primary flow pressure **[2]**.

The physical process inside the ejector and injector is also substantially different. Inside the ejector, a shock wave train occurs from the nozzle exit to the mixing chamber, and its structure, such as the shock wave length and expansion angle, affects the ejector's performance **[5–7]**. With the injector, especially the widely utilized steam-water injector, there is direct contact condensation between the steam and water, and a condensation shock occurs within the mixing chamber **[2]**. Moreover, the steam-water interface plays an important role for heat, mass and momentum exchange **[8]**. The steam jet may also transit from being stable to divergent and it exhibits diverse patterns **[9]**. Regarding the history of ejectors and its current applications and development, the readers may refer to review papers written by Elbel **[10]**, Besagani et al. **[1]**, Chen et al. **[11]**, etc. Moreover, the injector, as a passive jet pump, is extensively used in numerous industrial applications **[8]**. Since it has significant heat exchange abilities, it is presently being investigated for utilization as a passive cooling system for light water reactors **[2]**.

To further enhance the understanding of its physical process and performance, a substantial amount of studies are based on zero or one dimensional ejector modelling **[1]**. In the 1950s, Keenan and Neumann **[12]** introduced a constant-pressure mixing model, and later added a constant-area mixing model. Eames et al. **[13]** expounded on the friction loss inside the injector, and conducted an experiment to validate their own model. Shen et al. **[14]** proposed an optimization design methodology for the ejector. Munday and Bagster **[15]** further developed the constant-pressure mixing model by assuming that the primary fluid fans out and forms a ‘‘hypothetical -throat” prior to mixing with the entrained fluid, and offered a semi-empirical formula. Huang et al. **[16]**

performed a 1D analysis regarding ejector performance by assuming double-choking before mixing both the primary and secondary flow, which was widely employed in later research. Zhu et al. **[17]** proposed a 2D expression for velocity distribution, so as to approximate the viscosity flow on the cross section of the ejector, by introducing a ‘‘shock circle’’ at the entrance of the constant area mixing chamber. In all of the above modelling, the irreversible loss is usually taken by selecting isentropic coefficients for the primary flow nozzle, secondary flow nozzle, and the diffuser, with typical values ranging from 0.8 to 0.95 **[16,18,19]**. The irreversible loss of momentum inside the mixing chamber is also assessed by another coefficient, namely, the mixing loss coefficient, with a typical value from 0.7 to 0.9 **[16,18,19]**. It is assumed that critical flow is reached at the nozzle throat **[16,17,18]**.

For the steam–water injector, different modelling approaches have been applied. Usually, empirical coefficients are involved, which are limited in their usage. In order to predict the exit pressure at the steam nozzle, numerous methods were proposed. Cattadori et al. **[20]**, Yan et al. **[4]**, and Zhang et al. **[21]** utilized empirical relations obtained from their experiments. Li et al. **[22]** assumed an isentropic process within the steam nozzle, while Trela et al. **[23]** multiplied a coefficient on the velocity value that was calculated from the isentropic process. Narabayashi et al. **[24]** assumed that critical flow is attained at the steam nozzle exit, and they employed another empirical relation to calculate the critical pressure at the steam nozzle exit.

Similar to the steam nozzle, the calculation of the water nozzle also involves empirical relations. Cattadori et al. **[20]** assumed the exit pressure at the water nozzle

equals the steam pressure at the steam nozzle exit, which is the same as the ejector. Beithou and Aybar **[25]**, and Trela et al. **[23]** also made the same assumption. Yan et al. **[4]** provided an empirical relation for computing the pressure at the water nozzle exit, while Zhang et al. **[21]** provided another empirical relation.

Since the condensation primarily occurs inside the mixing chamber, numerous models have been proposed to take this phenomena into consideration. Deberne et al. **[26]** developed a simple model of the mixing section and the shock wave, which requires one empirical closure equation. Beithou and Aybar **[25]** designed a mathematical modeling of the steam-driven jet pump without condensation shock, in which a condensation profile was utilized; however, they did not take the mixing loss into account. Yan et al. **[4]** adopted the same approach as Beithou and Aybar **[25]**, yet they took the mixing loss into consideration with an empirical coefficient. Trela et al. **[23]** used an empirical heat transfer correlation to calculate the exit temperature of the mix nozzle. Furthermore, Deberne et al. **[26]** assumed that steam and liquid have the same pressure value inside the mixing nozzle; thus, they used an equivalent pressure obtained from an empirical relation of the condensation rate to calculate the mixing nozzle pressure. Li et al. **[22]** also utilized an empirical correlation of the condensate rate, in order to determine the fluid state inside the mixing nozzle. Other models, however, are more complex. These used a 2D approach or two phase model, with a two or three fluid approach. Narabayashi et al. **[24]** conducted an analytical and experimental study on water-steam injectors. The authors utilized a 2D axisymmetric and steady state formulation, where phases were treated as separate, homogeneous and immiscible.

Manno and Dehbi **[27]** divided the mixing nozzle into two flow regimes, separated flow and dispersed flow, and developed a separate mathematical model for each. Recently Heinze et al. **[28]** utilized a one-dimensional three-fluid model for the direct condensation of steam jets in flowing water. In the diffuser of the steam-water injector, a single phase water flow was taken and Bernoulli's equation was adopted to model the process **[2]**. All the researchers included a certain loss coefficient in their models.

However, in all the above-mentioned studies on steam-water injectors, detailed analyses on the different sections of the steam nozzle are rare. Although a critical flow condition is assumed, the fluid state at the nozzle throat was not given. These studies often utilized empirical relations to compute the steam nozzle exit pressure, which is quite limited. In this paper, the converging and diverging sections of the steam nozzle will be thoroughly investigated. Additionally, the pressure and temperature at the nozzle throat will be calculated, based on the local sound velocity reached at critical flow conditions. This approach, which was used by Liu et al. when predicting an ejector **[29]**, will provide a better method by which to calculate the nozzle exit pressure.

Furthermore, exergy analysis is crucial for evaluating the efficiency related to ejector performance enhancement **[18,30,31,32]**. However, limited studies are focused on the injector. Trela et al. **[33]** conducted as exergy analysis of a two-phase steam-water injector; they pointed out that the exergy efficiency of the injector can be quite high, from 27% to 45%.

Moreover, the injector can be utilized in district heating systems, because of its compact size and no need for external energy. Since the injector can be used as a pump

in district heating systems driven with high pressure steam to replace conventional electric-driven pumps, it is a viable alternative for reducing electricity cost. Yan et al. **[4]** experimented on the performance of a steam-driven jet injector with a high inlet water temperature (maximum 341.15 K) for a district-heating system and analyzed the effect of the inlet steam pressure, inlet water pressure and temperature on injector performance. They ascertained that the lifting-pressure coefficient was significantly affected by the nozzle throat area of the mixing chamber. However, no other geometric parameters were discussed; neither was an exergy analysis performed.

First, a one-dimensional mathematical model of the steam-water two-phase injector was developed, in which an iterative calculation of the speed of sound at the throat of the steam nozzle was conducted to determine the pressure at the nozzle throat, and hence, the steam mass flow rate. Then the nozzle exit pressure was computed, based on the fluid state at the nozzle throat. The mixing chamber was treated with a lump method, so as to simplify the model. Moreover, the irreversible losses inside the injector were also considered. Second, the model was validated with experimental data from Yan et al. **[4]**. Thirdly, based on the validated model, the influences regarding the different area ratios on injector performance used in district heating systems from Yan's paper were thoroughly investigated. Finally, exergy destruction rates were also computed for each component of the injector, and the exergy efficiency was obtained at different area ratios and pressures. Real fluid was adopted in the modelling protocol. In this context, the main objectives of this contribution are to **(i)** propose and validate a simplified model for a steam-water injector, which provides a superior method to calculate the steam

nozzle exit pressure, **(ii)** optimize the geometric parameters of an injector used for district heating, which will be beneficial toward improving its performance, **(iii)** perform an exergy analysis of the injector and calculate its exergy efficiency under various inlet conditions and area ratios, so as to supplement an understanding of the injector.

2. Modelling of injector

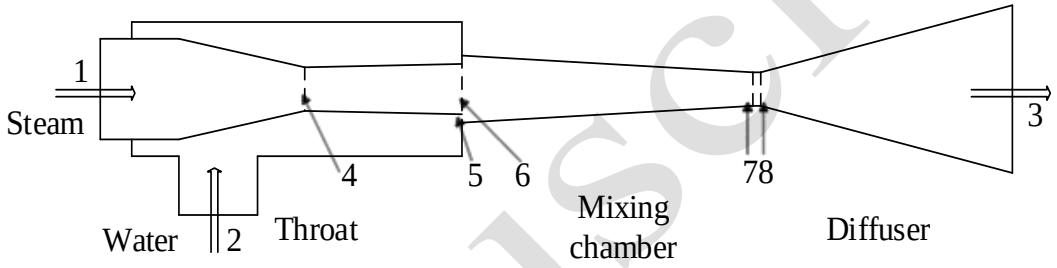

Fig. 1. Schematic of steam-water injector with state points.

Fig. 1. illustrates the schematic diagram of an injector. The primary flow enters the nozzle and accelerates. At the exit of the diverging section of the steam nozzle, a rather low pressure region is created to entrain the secondary flow – supercooled water **[2]**. Due to the temperature and velocity difference, the transportation of heat, mass and momentum occur between the steam and water at the mixing chamber, resulting in a pressure increase and velocity decrease. The steam is gradually condensed and becomes completely subcooled water at the end of the mixing section after the shock wave. Once at the diffuser the water's kinetic energy is partially converted into a further pressure increase.

There are three diverse operational modes for an ejector: critical mode, subcritical mode and backflow mode. The entrainment ratio is defined as the mass flow ratio between the secondary flow and primary flow, varying with back pressure (or condenser pressure), as depicted in **Fig. 2**. The three operational modes also exist for an injector.

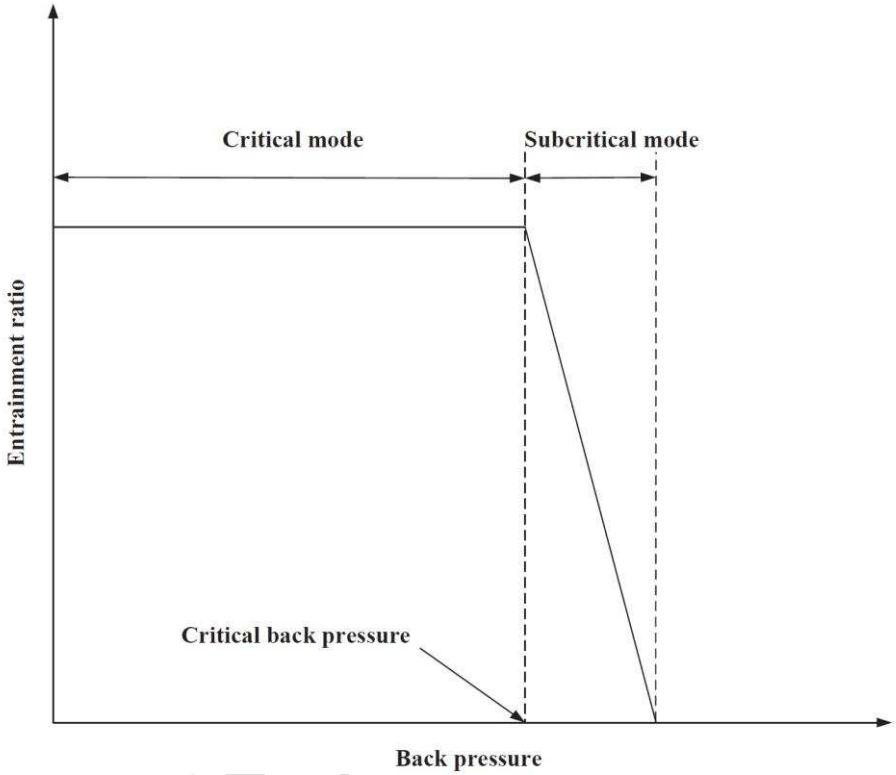

Fig. 2. Three operational modes of ejector.

A model for the steam-liquid injector can be established by using the following assumptions:

1. The injector operates at critical model. The flow inside the injector is a steady, homogenous and one dimensional flow.
2. At the nozzle throat, the flow reaches the critical flow condition, which means that the sound velocity is reached there.
3. The isentropic efficiency of the converging and diverging sections of motive

nozzle, η_1 and η_2 are given.

4. The inlet steam is superheated and the inlet flow velocity is neglected for both steam and water.
5. The heat transfer between the fluid and wall is neglected.
6. The gravitational force effect on the flow is neglected.

2.1 Motive nozzle

At the motive nozzle the steam is taken as a real fluid, the intermolecular interactions are considered, and the ideal-gas equation is viewed as not applicable. The computational formula of steam is derived from IAPWS-IF97 and it reaches sonic velocity.

$$\eta_1 = \frac{h_1 - h_4}{h_1 - h_{4,is}} \quad (1)$$

$$h_{4,is} = f(P_4, s_1) \quad (2)$$

$$h_1 = h_4 + \frac{u_4^2}{2} \quad (3)$$

$$\mathrm{C} = f(P_4, h_4) \quad (4)$$

By assuming a value for pressure P_4, h_4 can be determined from inlet entropy s_1 and pressure P_4. Thus, enthalpy h_4 can be calculated for a specific motive nozzle isentropic efficiency η_1. The value of η_1 was 0.9, as recommended by **[16]**. The energy conservation between the inlet and the throat of the motive nozzle can be expressed as depicted in **Eq. (3)**, in order to calculate velocity u_4. According to pressure P_4 and the calculated enthalpy h_4, the speed of sound C at the nozzle throat can also be adequately

determined. Next, after comparing the calculated velocity u_4 to the speed of sound C, if the relative correlation error between u_4 and the speed of sound C is greater than 0.1%, pressure P_4 is continuously updated, until the iteration provides a reasonable agreement **[29]**. In the present calculation from **Eq. (4)**, the results show that the vapor is still superheated at the nozzle throat, so the fluid is single phase and the sound velocity is well-defined. But when the inlet (motive) steam is saturated or only slightly superheated, it becomes wet before it reaches the throat, which often occurs in practical application of ejectors. Wet steam is two-phase medium, for which "sound velocity" is dispersive and can be described by several different models. Software such as CoolProp, does not return a value in this two-phase region. In such case, the method proposed here can still be applied but the user should be warned that the velocity C, as well as other properties, should be custom-calculated from suitably defined state equations.

For a given throat area A_4, the steam mass flow rate can be calculated based on mass conservation equation:

$$\dot{m}_1 = \rho_4 A_4 u_4 \tag{5}$$

While the flow density at the nozzle throat is calculated as follows:

$$\rho_4 = f(P_4, h_4) \tag{6}$$

The mass and energy equations of the divergent section of motive nozzle are:

$$\dot{m}_1 = \rho_6 A_6 u_6 \tag{7}$$

$$h_6 + \frac{u_6^2}{2} = h_4 + \frac{u_4^2}{2} \tag{8}$$

$$\eta_2 = \frac{h_4 - h_6}{h_4 - h_{6,is}} \tag{9}$$

The isentropic efficiency η_2 is assumed to be equal to η_1.

$$h_{6,is} = f(P_6, s_4) \tag{10}$$

$$\rho'_6 = f(P_6, h_6) \tag{11}$$

By assuming a value for the pressure P_6, density ρ_6 that was calculated from **Eq.** (**7**) was then compared to the density ρ'_6 calculated from **Eq.** (**11**), while the exit pressure, P_6, is updated until the iteration provided a reasonable agreement.

2.2 Suction nozzle

In this paper the secondary flow is liquid, and the exit pressures of steam nozzle P_5 and water nozzle P_6 were assumed to be equal.

$$P_5 = P_6 \tag{12}$$

$$\frac{u_5^2}{2} = \xi_1 \left(\frac{P_2}{\rho_2} - \frac{P_5}{\rho_5}\right) \tag{13}$$

$$h_5 + \frac{u_5^2}{2} = h_2 \tag{14}$$

Here, ξ_1 depicts the pressure loss coefficient within water nozzle and is empirically determined as ($\xi_1 = 0.9$) **[21]**. According to the overall condition of the suction nozzle, the exit velocity u_5 and enthalpy h_5 can be obtained by using **Eqs. (13)** and **(14)**.

$$\dot{m}_2 = \rho_5 A_5 u_5 \tag{15}$$

2.3 Mixing chamber

The mixing chamber is a converging chamber, whereby the steam jet is directly

condensed in subcooled water and the two flow steams reach the same speed. Moreover, the non-condensed steam percentage decreases along with the increase of the length of the mixing section; thus, a normal shock wave is then induced at the end of this mixing chamber. Next, the steam becomes completely subcooled water at the end of the mixing section **[4]**. Though the mixing chamber was treated separately in most previous studies, in order to simplify the calculation and avoid unknown variables, the inject steam nozzle, water nozzle and the mixing chamber were considered as a control volume. The mass and energy equations are presented as follows:

$$\dot{m}_1 + \dot{m}_2 = \rho_8 A_8 u_8 \tag{16}$$

$$\dot{m}_1 h_1 + \dot{m}_2 h_2 = (\dot{m}_1 + \dot{m}_2)\left(h_8 + \frac{u_8^2}{2}\right) \tag{17}$$

$$\rho_8' = f(P_8, h_8) \tag{18}$$

At the proximity of the exit plane of the mixing section, the fluid will be in a liquid state. Hence, through the above formulation, the complex modelling procedure for mixture quality and condensation can be avoided, which considerably simplifies the computation. This kind of approach was utilized by Zhao et al. **[32]** when predicting the diffuser section of an ejector.

Furthermore, the momentum equation was utilized for the mixing chamber only, where coefficient β was the momentum correction factor, with a value of 0.75 **[34]**.

$$\beta(P_5 A_5 + P_6 A_6 + \dot{m}_1 u_6 + \dot{m}_2 u_5) = P_8 A_8 + (\dot{m}_1 + \dot{m}_2) u_8 \tag{19}$$

2.4 Diffuser

In the diffuser, the kinetic energy of the mixing stream will then be converted into

a static pressure increase.

$$\dot{m}_1 + \dot{m}_2 = \rho_3 A_3 u_3 \tag{20}$$

$$\frac{u_8^2}{2} + \frac{P_8}{\rho_8} = \frac{P_3}{\rho_3} + \frac{u_3^2}{2} + h_L \tag{21}$$

where h_L is the head loss which is given **[35]**.

$$h_L = \frac{u_8^2}{2}\left[1 - \left(\frac{A_8}{A_3}\right)^2 - C_p\right] \tag{22}$$

where C_p represents the pressure recovery coefficient.

$$C_p = \frac{P_3 - P_8}{P_{3th} - P_8} \tag{23}$$

P_{3th} depicts the pressure of the diffuser outlet for cases where there is no loss.

The energy balance is laid out for the entire injector **[32]**.

$$\dot{m}_1 h_1 + \dot{m}_2 h_2 = (\dot{m}_1 + \dot{m}_2)\left(h_3 + \frac{u_3^2}{2}\right) \tag{24}$$

Moreover, density ρ_3, is determined from pressure p_3 and enthalpy h_3. The entire computation protocol for the injector is detailed in **Fig. 3**. In this way the calculation of the steam nozzle was altered, and calculation of the speed of sound at the steam nozzle throat is performed. Furthermore, the nozzle exit pressure has been more precisely predicted than with previously reported methods. The formulation approach for ejector modelling used by Zhao et al. **[32]** were adopted to simplify the injector computation, which is quite useful and reliable for practical engineering applications.

Both steam and water were treated as real fluids and CoolProp **[36]** was employed to compute their physical properties at various stated points or stages.

3. Results and discussions

The experimental data published by Yan et al. was used to validate the proposed numerical model **[4]**. The parameters of steam, water and injector configuration from Yan et al. **[4]** is shown in **Table 1**.

Table 1
Parameters of steam inlet, water inlet and injector configuration

Inlet steam pressure, $\mathbf{P_1}$	0.2-0.6 MPa
Inlet steam temperature, $\mathbf{T_1}$	433.15 K
Inlet water pressure, $\mathbf{P_2}$	0.14-0.49 MPa
Inlet water temperature, $\mathbf{T_2}$	291.15 K
Steam nozzle throat diameter, $\mathbf{D_4}$	26 mm
Steam nozzle outlet diameter, $\mathbf{D_6}$	30 mm
Water nozzle outlet area, $\mathbf{A_5}$	196.5 mm^2
Mixing chamber throat diameter, $\mathbf{D_8}$	18 mm
Diffuser outlet diameter, $\mathbf{D_3}$	100 mm

3.1 Model validation: Pressure profiles of injector

Tables 2 and **3** identify the pressure profiles and error ratios, while **Figs. 4** and **5** display the pressure profiles at different cross-sections within the injector, under different inlet steam pressures and inlet water pressures, respectively. In Yan's experiment, when the inlet steam pressure varied from 0.2 MPa to 0.6 MPa, the diffuser exit pressure increased from 0.4 MPa to 0.96 MPa and from 0.44 MPa to 1.04 MPa, which precisely correlates with the present calculation. They agree quite well, with a maximum error of 9.5%. In Yan's experiment, when the inlet water pressure varied from 0.14 MPa to 0.49 MPa, the diffuser exit pressure increased from 0.52 MPa to 0.69 MPa and from 0.54 MPa to 0.73 MPa, which is also consistent with the present calculation.

The maximum error was 8.9%. The trends and calculated data from **Figs. 4** and **5** are similar for both experiments; however, the results proved that the current model can more adequately predict the injector parameters.

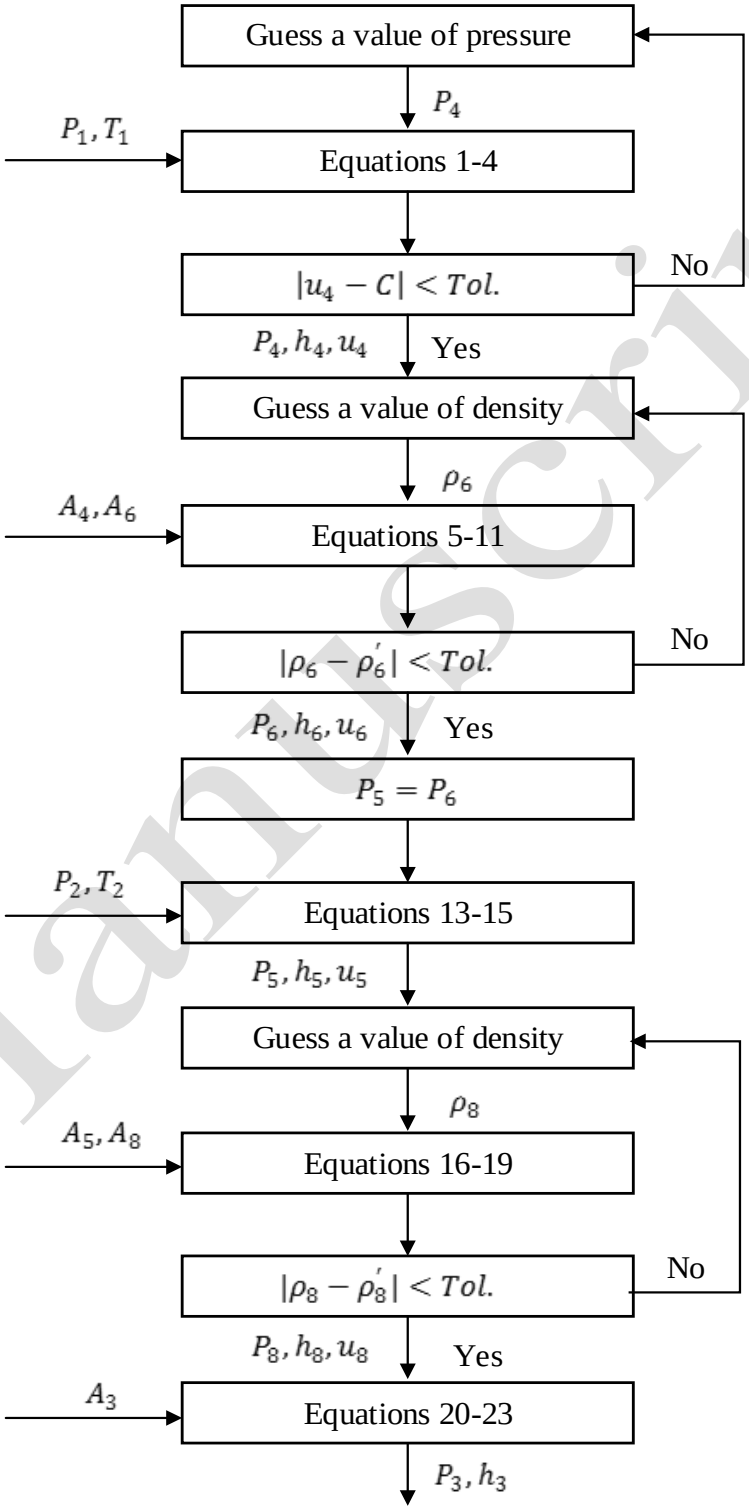

Fig. 3. Computational procedure of steam-water injector.

Table 2

The pressure profiles for different inlet steam pressures ($T_2 = 291.15\ K,\ p_2 = 0.23\ MPa,\ D_4 = 18mm$)

	Steam nozzle inlet (MPa)	Steam nozzle throat (MPa)	Steam nozzle outlet (MPa)	Mixing chamber outlet (MPa)	Diffuser outlet (MPa)
Experiment	0.2	/	0.049	0.34	0.4
Calculation	0.2	0.134	0.048	0.36	0.438
Error ratio	/	/	2.04%	5.96%	9.5%
Experiment	0.3	/	0.069	0.48	0.554
Calculation	0.3	0.15	0.070	0.51	0.590
Error ratio	/	/	1.45%	6.25%	6.5%
Experiment	0.4	/	0.096	0.66	0.71
Calculation	0.4	0.2	0.09	0.68	0.74
Error ratio	/	/	6.25%	3.03%	4.23%
Experiment	0.5	/	0.122	0.8	0.85
Calculation	0.5	0.24	0.12	0.84	0.89
Error ratio	/	/	1.64%	5.0%	4.71%
Experiment	0.6	/	0.14	0.92	0.96
Calculation	0.6	0.29	0.14	0.99	1.04
Error ratio	/	/	0.0%	7.61%	8.33%

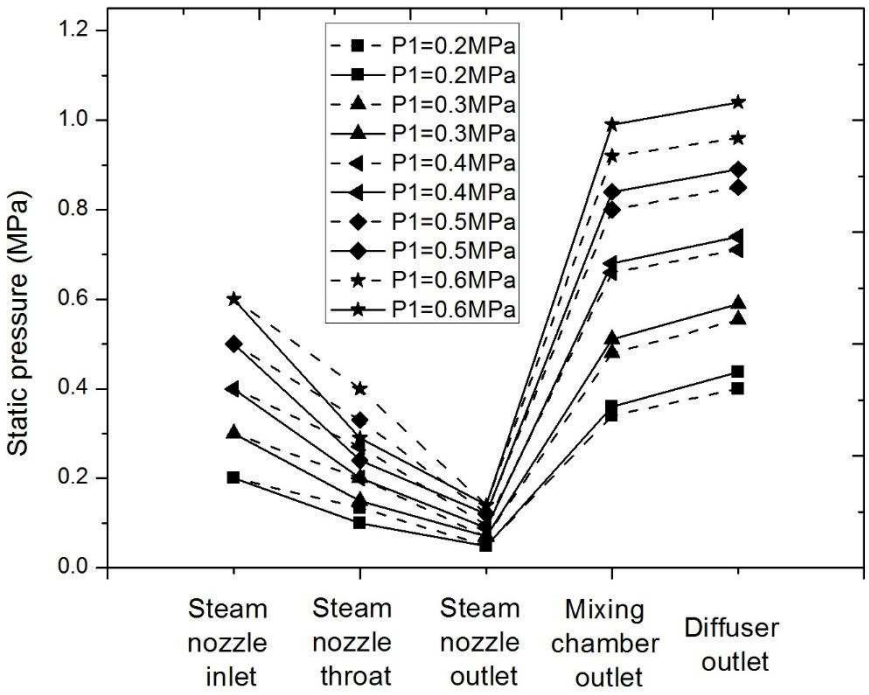

Fig. 4. Pressure profiles for different inlet steam pressures ($T_2 = 291.15\ K,\ p_2 = 0.23\ MPa, D_4 = 18mm$,

dashed line-experiment, solid line-calculated)

Table 3

Pressure profiles for different inlet water pressures ($T_2 = 291.15\ K,\ p_1 = 0.3\ MPa,\ D_4 = 18mm$).

	steam nozzle inlet (MPa)	steam nozzle throat (MPa)	steam nozzle outlet (MPa)	mixing chamber outlet (MPa)	diffuser outlet (MPa)
Experiment	0.3	/	0.071	0.47	0.52
Calculation	0.3	0.149	0.072	0.5	0.54
Error ratio	/	/	1.41%	6.38%	3.85%
Experiment	0.3	/	0.073	0.48	0.554
Calculation	0.3	0.15	0.072	0.51	0.590
Error ratio	/	/	1.37%	6.25%	6.5%
Experiment	0.3	/	0.075	0.49	0.6
Calculation	0.3	0.15	0.072	0.53	0.63
Error ratio	/	/	4.00%	8.16%	5.00%
Experiment	0.3	/	0.079	0.51	0.69
Calculation	0.3	0.15	0.072	0.55	0.73
Error ratio	/	/	8.86%	7.84%	5.80%

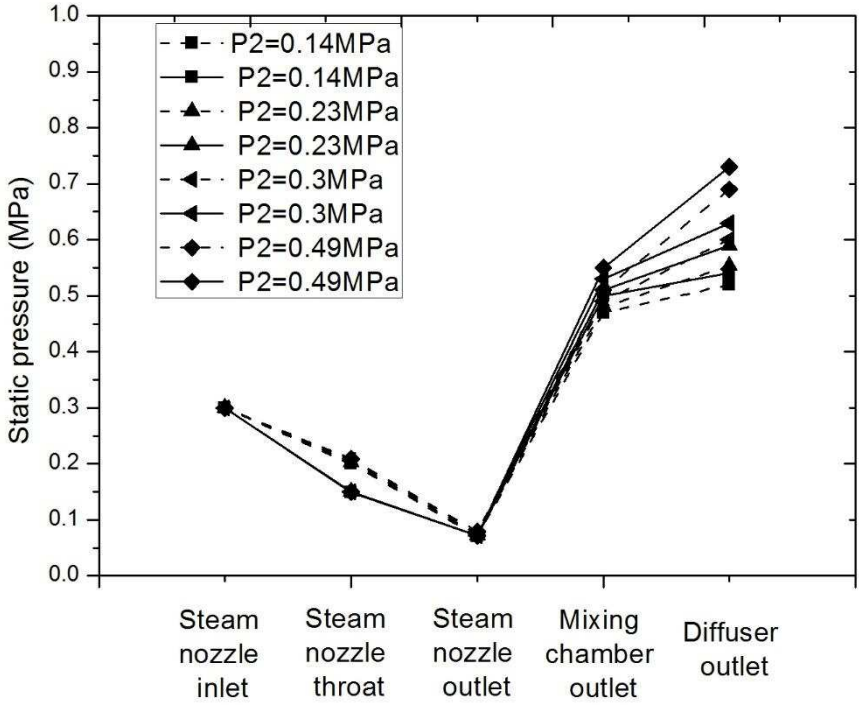

Fig. 5. Pressure profiles for different inlet water pressures ($T_2 = 291.15\ K, p_1 = 0.3\ MPa, D_4 = 18mm$, dashed line-experiment, solid line-calculated).

3.2 Model prediction: entrainment ratio

In the paper of Yan et al. **[4]**, the jet coefficient used was the value of the inlet water mass flux vs. the inlet steam mass flux. The jet coefficient can also be referred to as the entrainment ratio, which is the ratio of the mass flux of secondary flow – water vs. the mass flux of primary flow –steam, most often used by most researchers. The entrainment ratio is also an important index to measure the overall performance of the ejector and injector.

$$\omega = \frac{\dot{m}_2}{\dot{m}_1} \tag{25}$$

In the study from Yan et al. **[4]**, they only studied how the jet coefficient (entrainment ratio) varied with inlet water and steam pressure, but they did not examine how it changed with area ratios. This paper investigated the influence of area ratio A4/A7 on the entrainment ratio. **Fig. 6** illustrates the relationships between the entrainment ratio and area ratio from the predicted values according to the present model.

The entrainment ratio decreased with the increase of area ratio A4/A7. This is because, along with the increase of area ratio A4/A7 there was a slight increase of the inlet steam mass flux and a much higher decrease of inlet water mass flux, as demonstrated in **Fig. 7**.

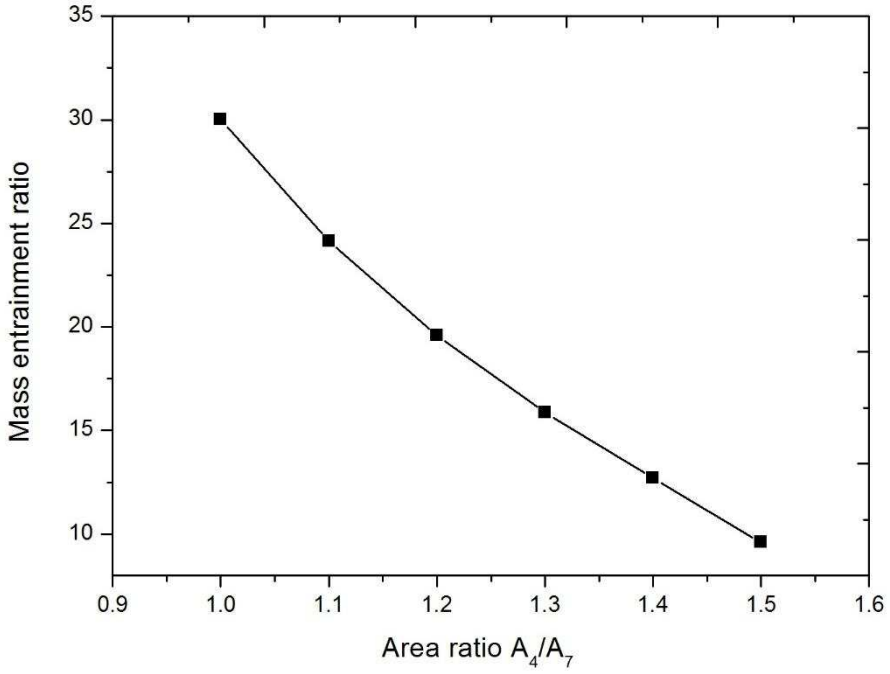

Fig. 6. Calculated entrainment ratio under different area ratio A_4/A_7

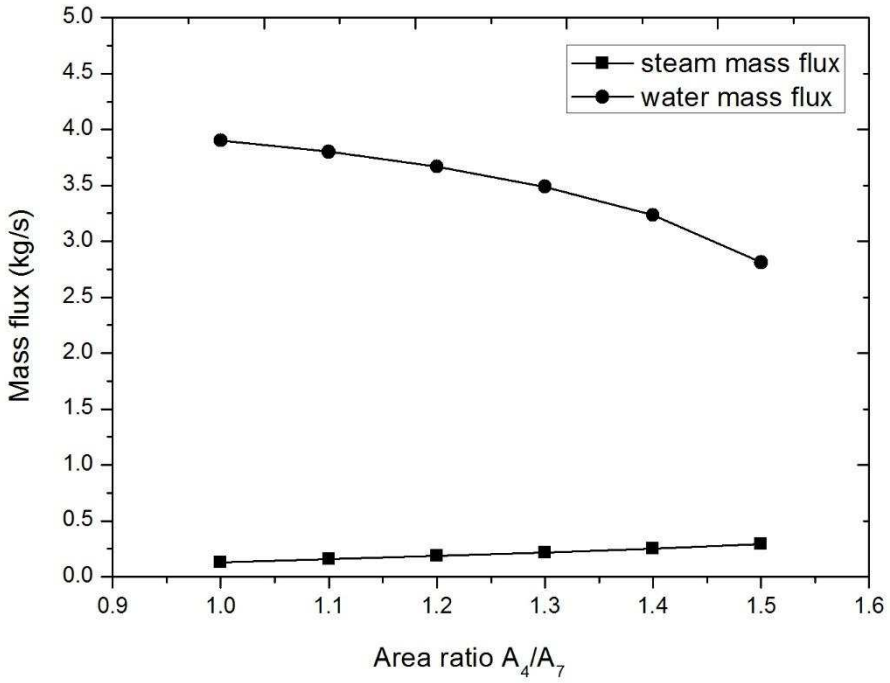

Fig. 7. Mass flux under different area ratio A_4/A_7

3.3 Model prediction: Influences of isentropic efficiency and loss coefficient on injector performance

Fig. 8 details how the entrainment ratio changes with the coefficient of isentropic efficiency. It can also be seen that η_1 has a more significant influence on the mass entrainment ratio than η_2. When η_1 increases from 0.75 to 0.95, the mass entrainment ratio drops from 19.1 to 15.07.

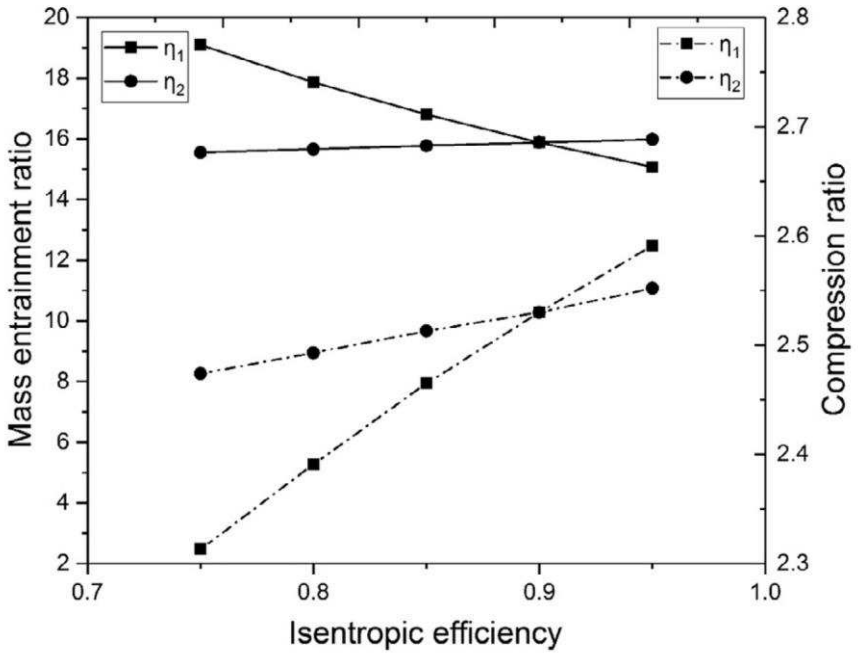

Fig. 8. Calculated entrainment ratio with coefficient of isentropic efficiency

However, in contrast, when η_2 varies from 0.75 to 0.95, the mass entrainment ratio only increases from 15.55 to 15.98. Thus,η_1 has an influence on both steam flux and water flux. Moreover, when η_1 increases, the steam flux will increase, and the exit pressure of the motive nozzle also increases rapidly, which causes the increase of the water nozzle exit pressure. Since these two pressures were assumed to be equal; accordingly, the exit velocity of the suction nozzle decreased sharply and the water flux dropped, which resulted in a lower mass entrainment ratio and a higher compression ratio. The outlet pressure of the motive nozzle and suction nozzle was slightly reduced

when η_2 increased, which led to a slight increase of exit velocities for both the motive nozzle and suction nozzle. Thus, the entrainment ratio reflects a limited increase; however, the compression ratio shows a more substantial increase than the entrainment ratio, because there is a square relationship that exists between mass flux and velocity.

Figs. 9 and **10** demonstrate the relationships between the entrainment ratio and loss coefficients of the suction nozzle and mixing chamber, respectively. The velocity of the suction nozzle rises when the loss coefficient increases, which correlates to a larger flow rate under a constant area and an increase in the mass entrainment ratio. The increase of the loss coefficient inside the mixing chamber will increase the injector outlet pressure (**Fig. 10**).

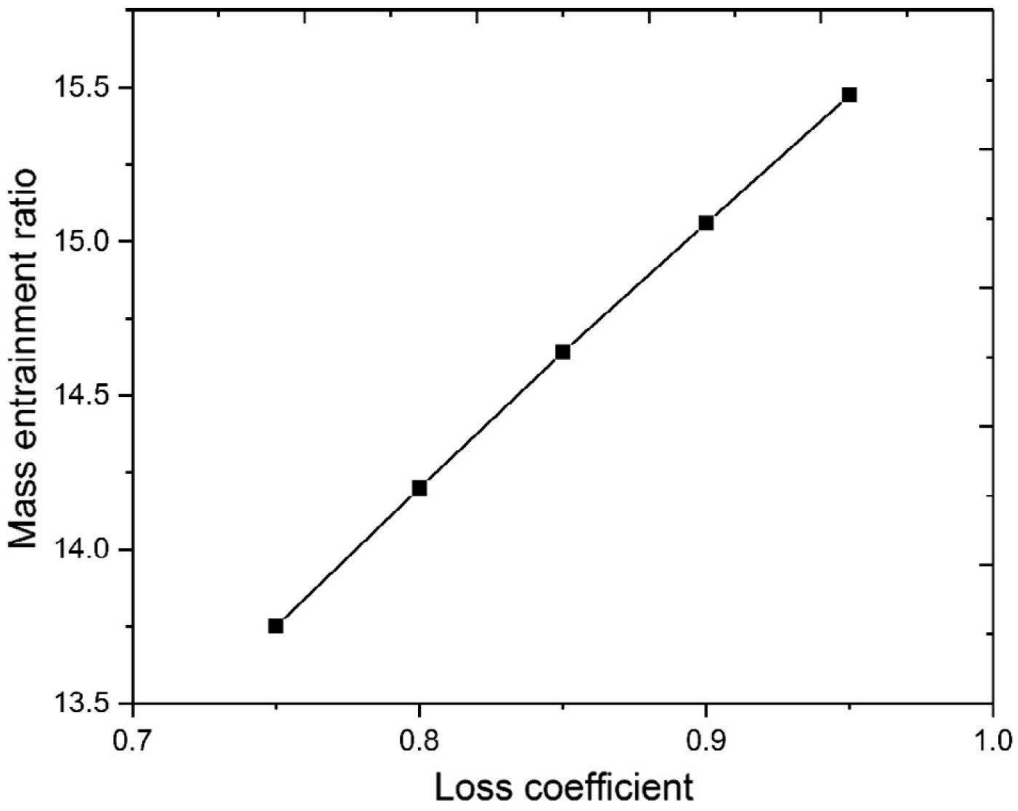

Fig. 9. Entrainment ratio with loss coefficient of suction nozzle

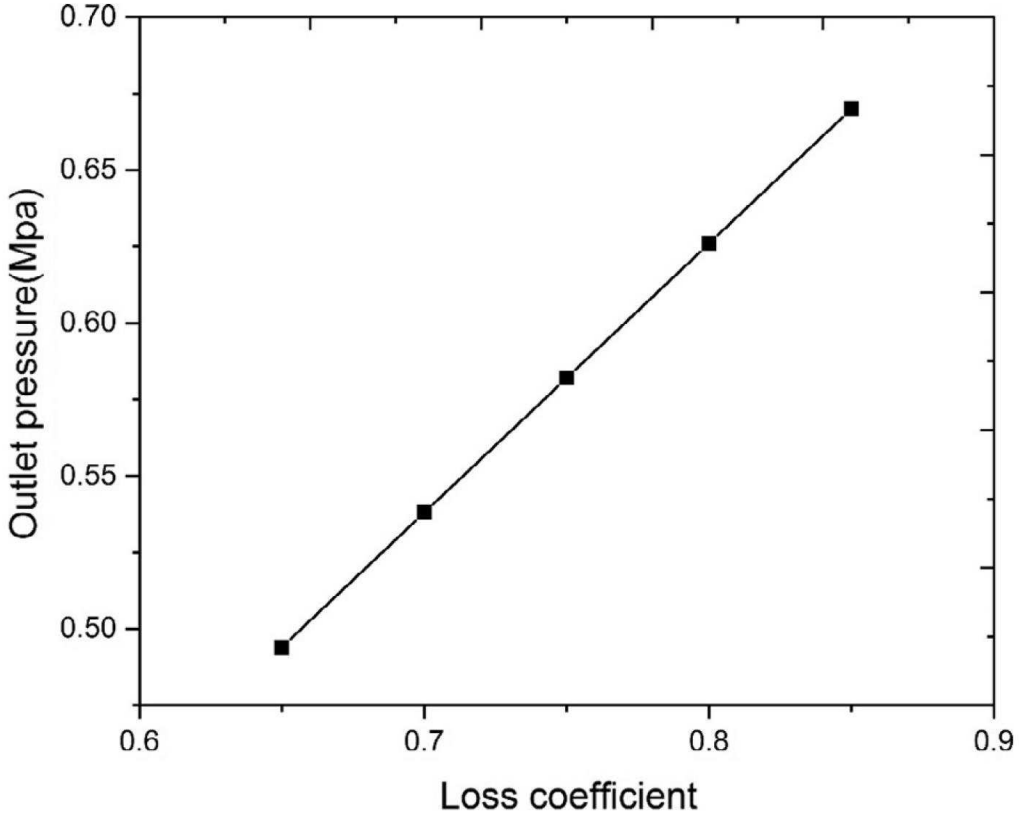

Fig. 10. Entrainment ratio with loss coefficient of mixing chamber

3.4 Model prediction: Compression ratio

In the study conducted by Yan et al. **[4]**, the lift pressure coefficient was used, which is the ratio of injector discharge pressure vs. the steam inlet pressure. However, the compression ratio is more often used by most researchers, which is the ratio of the injector discharge pressure vs. the water inlet pressure, which is another important index to measure the injector's performance. The influences of inlet steam and water pressure on the compression ratio are presented in **Fig. 11**.

$$\mathrm{R} = \frac{P_3}{P_2} \tag{26}$$

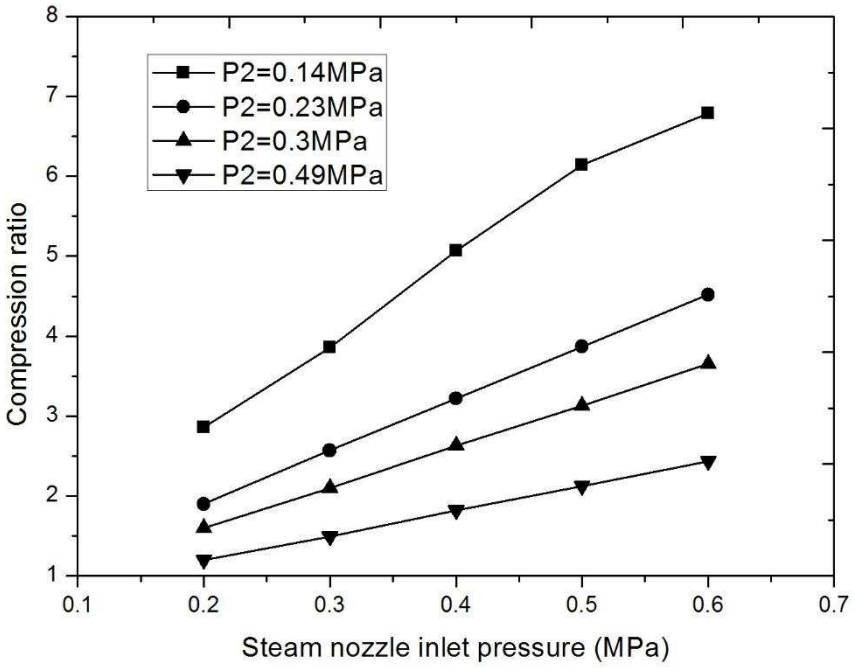

Fig. 11. Compression ratio under different steam and water inlet pressures.

The compression ratio increased in conjunction with the escalation of inlet steam pressure, but decreased along with the expansion of the inlet water pressure, because the increase of the inlet water pressure was much faster than that of the outlet water pressure. **Fig. 11** clearly shows that the compression ratio increased much more rapidly under a lower inlet water pressure and a higher inlet steam pressure.

3.5 Model prediction: Influences of area ratio on injector performance

The geometry of the injector has a significant influence on the performance of the injector, especially with regard to the area around the throat of the motive steam nozzle, the throat of the mixing chamber and the outlet of the diffuser. In order to simplify the

analysis, A7 is constant, thus, A4 is always considered as a variable. The pressure of the injector is shown in **Fig. 12** under different area ratios.

As can be ascertained from **Fig. 12**, the pressure of the injector increases under the increase of area ratio A4/A7, because the pressure is boosted mainly within the mixing chamber where the shock wave occurs. Moreover, the change of A4 will alter the velocity outlet of the steam nozzle; hence, affecting the mixing process. However, the process occurs inside the diffuser; thus, it cannot be transferred to the upstream and has no influence on pressures from the nozzle inlet to the mixing chamber outlet. Because the change is relatively small in A7, it exhibits almost no influence on the diffuser outlet pressure.

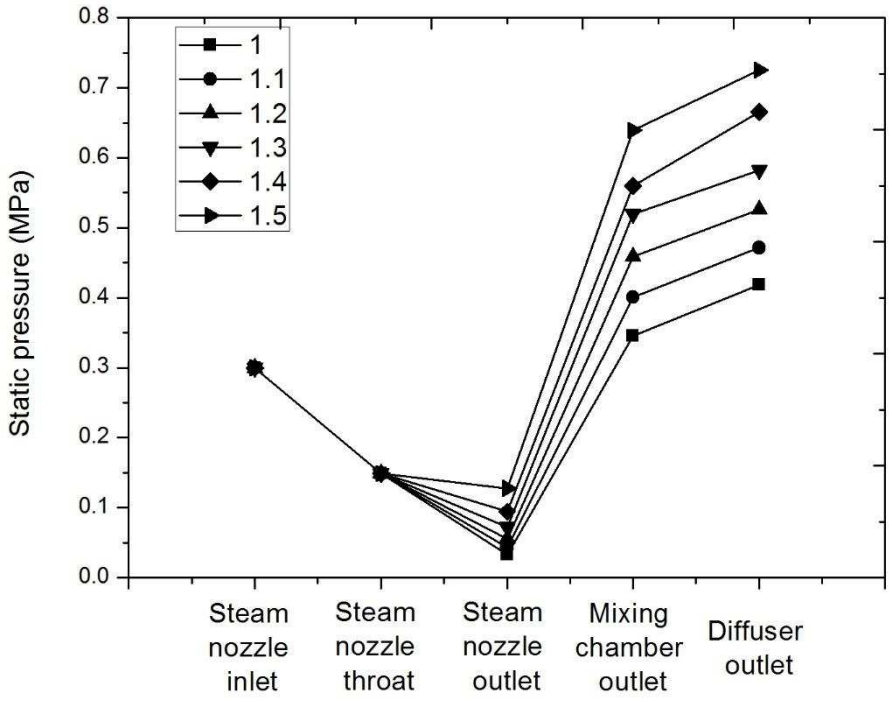

Fig. 12. Pressure under different area ratio A_4/A_7.

3.6 Model prediction: Exergy destruction rates & efficiency

The steam exergy:

$$\dot{E}_1 = \dot{m}_1 \left(h_1 - T_0 s_1 + \frac{u_1^2}{2} \right) \quad (27)$$

The water exergy:

$$\dot{E}_2 = \dot{m}_2 \left(h_2 - T_0 s_2 + \frac{u_2^2}{2} \right) \quad (28)$$

The outlet exergy:

$$\dot{E}_3 = (\dot{m}_1 + \dot{m}_2) \left(h_3 - T_0 s_3 + \frac{u_3^2}{2} \right) \quad (29)$$

Exergy destruction rates for each component are outlined in **Table 4**, and the detailed derivations of these equations may be retrieved from Lawrence and Elbel **[31]** and Yan et al. **[30]**. The ambient temperature T_0 utilized in this study is 298.15 K.

Table 5 shows the exergy destruction rates of each component, while primary irreversibility occurs in the steam nozzle (41.34%) and mixing chamber (57.95%). This is because of the flow experience phase change, great velocity, and temperature change in these particular sections. Moreover, the mixing between these two flows facilitates friction loss within the mixing chamber.

Table 4
Relations of exergy destruction rates for each component.

Components	Exergy destruction rates
Steam nozzle	$I_{1-4} = \dot{m}_1(T_0(s_4 - s_1) - (h_4 - h_1))$
Water nozzle	$I_{2-5} = \dot{m}_2(T_0(s_5 - s_2) - (h_5 - h_2))$
Mixing chamber	$I_{4-6} = T_0\big((\dot{m}_1 + \dot{m}_2)s_6 - \dot{m}_1 s_4 - \dot{m}_2 s_5\big) - (\dot{m}_1 h_4 + \dot{m}_2 h_5 - (\dot{m}_1 + \dot{m}_2)h_6)$
Diffuser	$I_{6-3} = (\dot{m}_1 + \dot{m}_2)(T_0(s_3 - s_6) - (h_3 - h_6))$

Table 5
Exergy destruction rates and their ratios to the total exergy destruction rates

Components	Exergy destruction rates(kW)	Ratio (%)
Steam nozzle	52.839	41.34
Water nozzle	0.692	0.54
Mixing chamber	74.073	57.95
Diffuser	0.225	0.18

The exergy efficiency of the steam–water injector was calculated as:

$$\phi = \frac{\dot{E}_3}{\dot{E}_1 + \dot{E}_2} \tag{29}$$

The results are shown in **Figs. 13** and **14**. The exergy efficiency increased with the enlargement of area ratio A4 /A7, and decreased with the entrainment ratio. The results presented in **Fig. 14** indicate that the efficiency is the highest for low entrainment ratio values, and the efficiency varied from 50% to 37% when the mass entrainment ratio ranged from 9.6 to 30.

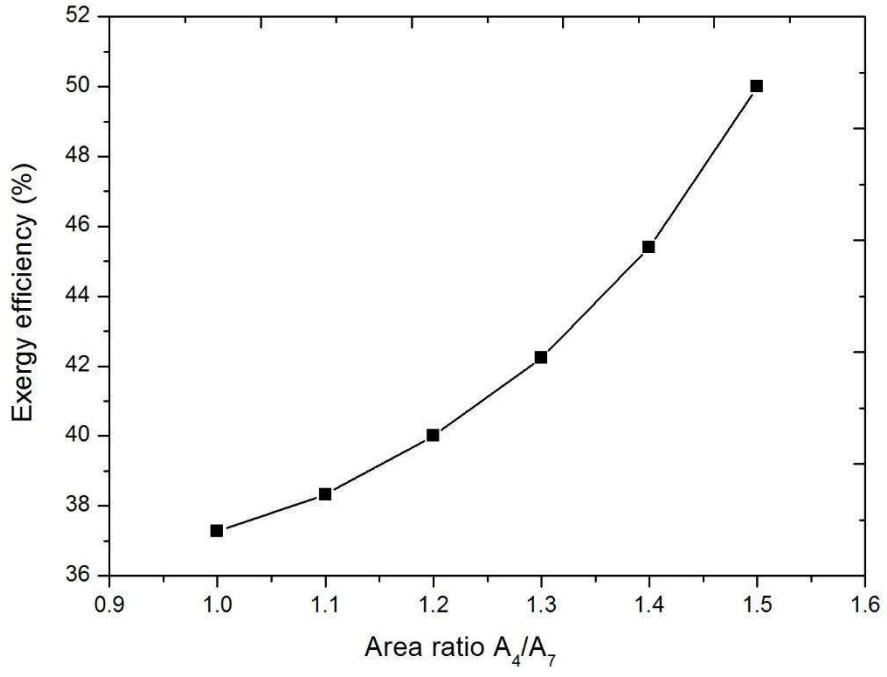

Fig. 13. Exergy efficiency under different area ratio A_4/A_7

Furthermore, the exergy efficiency also increased in coordination with the increase of inlet steam pressures, and decreased with the increase of inlet water pressures, as outlined in **Figs. 15** and **16**. The increase of inlet steam pressure led to the increasing exergy of the steam inlet nozzle and diffuser outlet, and the growth of outlet exergy was much quicker than inlet exergy. The inlet exergy increased in conjunction with the increase of inlet water pressures, while the exergy of the outlet decreased with the increase of inlet water pressure.

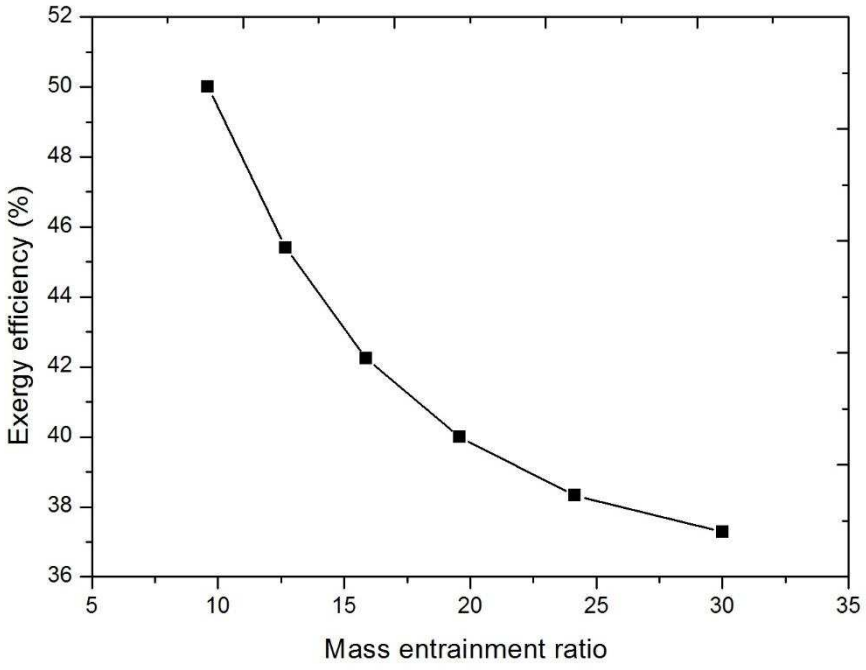

Fig. 14. Exergy efficiency versus mass entrainment ratio

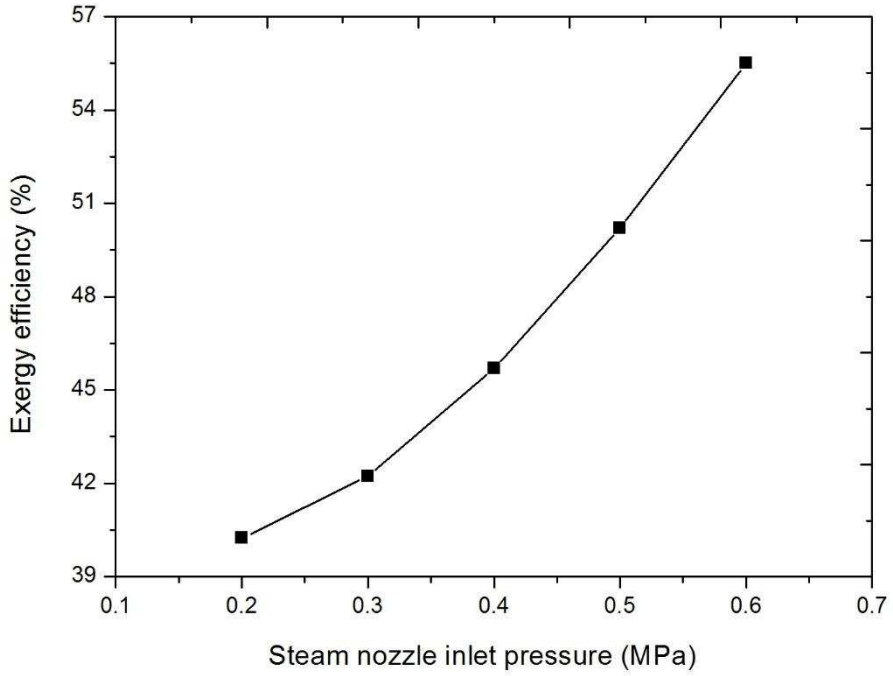

Fig. 15. Exergy efficiency under different inlet steam pressures ($p_2 = 0.23\ MPa$).

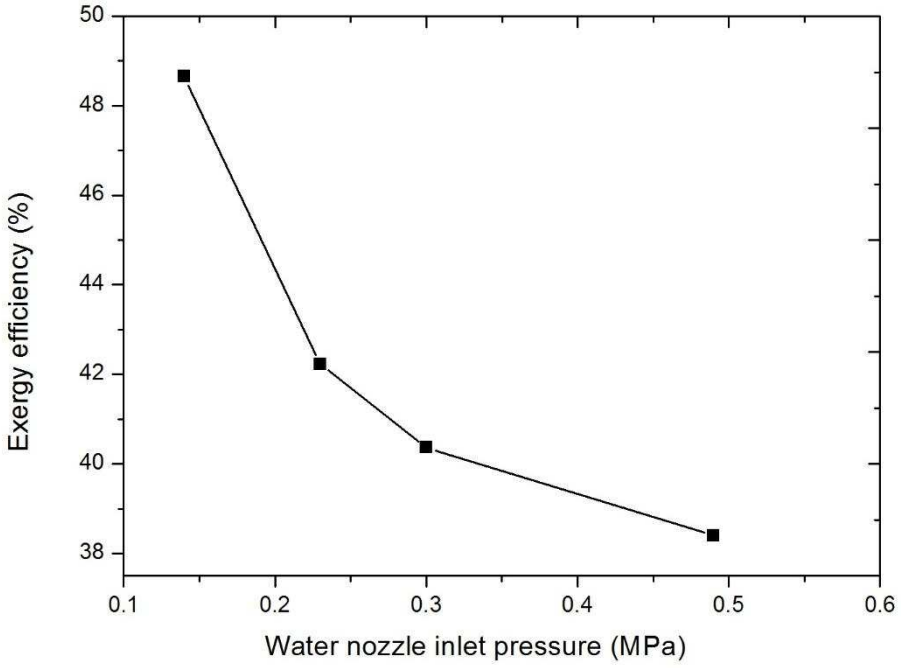

Fig. 16. Exergy efficiency under different inlet water pressures ($p_1 = 0.3\ MPa$)

4. Conclusion

A steam-liquid injector model was developed, which adopted a different approach

than existing models, so as to more precisely predict the motive nozzle exit pressure. The pressures inside the injector, while under different inlet steam and water pressures, were used to validate and confirm the model. The pressure of the diffuser exit varied from 0.438 MPa to 1.04 MPa, with inlet steam pressure from 0.2 MPa to 0.6 MPa and inlet water pressure from 0.14 MPa to 0.49 MPa, respectively. The calculation thoroughly and appropriately agrees with the experiment data, revealing a maximum relative error rate within 9.5%. This mathematical model was then utilized to adequately predict the performance of the steam-water injector by optimizing its geometry. Moreover, the exergy analysis was carried out, and the following conclusions were obtained:

(1) The compression ratio increases in proportion with the increase of inlet steam pressure, and decreases with the increase of inlet water pressure.

(2) The pressure of the injector increases precipitously under the increase of area ratio A4/A7.

(3) The isentropic efficiencies of the converging section and diverging section of the motive nozzle affect the entrainment ratio and compression ratio in a diverse manner. The increase of the former leads to the increase in the compression ratio and a decrease of the entrainment ratio, while the latter leads to the slight increase of both the compression and entrainment ratios.

(4) The exergy deterioration rates of each injector component were calculated, and the results reveal that the main irreversibility occurs within the steam nozzle (41.34%) and mixing chamber (57.95%). The exergy efficiency is the highest for low values

of the entrainment ratio. The exergy efficiency increases with the increase of inlet steam pressure and decreases with the increase of inlet water pressure.

Nomenclature

A	cross section area
C	speed of sound (m s^{-1})
C_p	pressure recovery coefficient
D	diameter (m)
$\dot{E}$	exergy
h	specific enthalpy (kJ kg^{-1})
h_L	head loss
I	exergy destruction rates (kW)
$\dot{m}$	mass flow rate (kg s^{-1})
P	pressure (MPa)
R	compression ratio
s	specific entropy (kJ kg^{-1} K^{-1})
T	temperature (K)
u	velocity (m s^{-1})

Greek letters

η	coefficient of isentropic efficiency
ρ	density
ω	entrainment ratio
ξ	loss coefficient
β	momentum correction factor
ϕ	exergy efficiency

Subscripts

is	isentropic
1-8	state points

References

[1] Besagni G, Mereu R, Inzoli F, Ejector refrigeration: A comprehensive review, Renew Sust Energ Rev 2016;53:373-407.

[2] Takeya Y, Shuichiro M, Hibiki T, Michitsugu M. Application of steam injector to improved safety of light water reactors. Progress in Nuclear Energy 2015;78:80-100.

[3] Wang X, Yu J. Experimental investigation on two-phase driven ejector performance in a novel ejector enhanced refrigeration system. Energy Convers Manage 2016;111:391-400.

[4] Yan JJ, Shao SF, Liu JP, Zhang Z, Experiment and analysis on performance of steam-driven jet injector for district-heating system. Appl Therm Eng 2005;25(8-9):1153-1167.

[5] Zhu Y, Wang Z, Yang Y, Jiang PX, Flow visualization of supersonic two-phase transcritical flow of CO2 in an ejector of a refrigeration system. Int J Refrig 2017;74: 352-359.

[6] Zhu Y, Jiang PX. Experimental and analytical studies on the shock wave length in convergent and convergent–divergent nozzle ejectors. Energy Convers Manage 2014;88: 907-914.

[7] Zhu Y, Jiang PX. Experimental and numerical investigation of the effect of shock wave characteristics on the ejector performance. Int J Refrig 2014;40:31-42.

[8] Zong X, Liu JP, Yang XP, Chen Y, Yan JJ. Experimental study on the stable steam jet in subcooled water flow in a rectangular mix chamber. Experimental Therm Fluid Sci 2015;75:249-257

[9] Yang XP, Liu JP, Zong X, Chong DT, Yan JJ. Experimental study on the direct contact condensation of the steam jet in subcooled water flow in a rectangular channel: Flow patterns and flow field. Int J Heat Fluid Flow 2015;56:172-181.

[10] Elbel S. Historical and present developments of ejector refrigeration systems with emphasis on transcritical carbon dioxide air-conditioning applications. Int J Refrig 2011;34(7):1545–61.

[11] Chen J, Jarall S, Havtun H, Palm B. A review on versatile ejector applications in refrigeration systems. Renew Sust Energ Rev 2015;49:67-90.

[12] Keenan JH. An investigation of ejector design by analysis and experiment. ASME J Appl Mech Trans 1950;72:299-309.

[13] Eames IW, Aphornratana S, Heider H. A theoretical and experimental study of small-scale steam jet refrigerator. Int J Refrig 1995;18:378-386.

[14] Zhang B, Shen SQ, Li HJ, Abudula A. Numerical study of ejector performance with two-dimensional flow model. Therm Sci Technol 2003;2(2):149-153.

[15] Munday JT, Bagster DF. A new ejector theory applied to steam jet refrigeration. Ind Eng Chem Process Des Dev 1977;16:442-449.

[16] Huang BJ, Chang JM, Wang CP, Petrenko VA. A 1-D analysis of ejector performance. Int J Refrig 1999;22:354-364.

[17] Zhu Y, Cai W, Wen W, Li Y. Shock circle model for ejector performance evaluation. Energy Convers Manage 2007;48(9):2533-2541.

[18] Chen J, Havtun H, Palm B. Investigation of ejectors in refrigeration system: optimum performance evaluation and ejector area ratios perspectives. Appl Therm Eng 2014;64:182-191.

[19] Bai T, Yan G, Yu J. Performance evolution on a dual-temperature CO2 transcritical refrigeration cycle with two cascade ejectors. Appl Therm Eng2017;120:26-35.

[20] Cattadori G, Galbiati L, Mazzocchi L, Vanini P. A single-stage high pressure steam injector for next generation

reactors: test results and analysis. Int J Multiph Flow 1995;21:591-606.
[21] Zhang Z, Chong D, Yan J. Modeling and experimental investigation on water-driven steam injector for waste heat recovery. Appl Therm Eng 2012;40:189-197.
[22] Li G, Huang YH, Lv Z, Huang HL. Research on mechanism of two phase flow lifting pressure equipment and output regulation. Adv Mater Res 2012;430-432:1619-1623.
[23] Mirbach T, Ohrem S, Schild S, Moser A. Analysis of application of feed water injector heaters to steam power plants. Pol Marit Res 2009;16:64-70.
[24] Narabayashi T, Nei H, Ozaki O, Shioiri A, Mizumachi W. Study on high-performance steam injector. 1st report. Development of analytical model for characteristic evaluation. Trans Jpn. Soc Mech Eng B 1999;62(597):155-162.
[25] Beithou N, Aybar NS. A mathematical model for steam-driven jet pump. Int J Multiph Flow 2000;26(10):1609-1619.
[26] Deberne N, Leone JF, Duque A, Lallemand A. A model for calculation of steam injector performance. Int J Multiph Flow 1999;25:841-855.
[27] Manno VP, Dehbi AA. A note: a model of steam injector performance. Chem Eng Commun 1990;95:107-119.
[28] Heinze D, Schulenberg T, Behnke L. A physically based, one-dimensional three-fluid model for direct contact condensation of steam jets in flowing water. Int J Heat Mass Transfer 2017;106:1041–1050.
[29] Liu F, Groll, Eckhard A. Analysis of a two phase flow ejector for transcritical CO_2 cycle. Int. Refrig. Air Conditioning Conference 2008; P.924:1-11.
[30] Yan G, Chen J, Yu J. Energy and exergy analysis of a new ejector enhanced auto-cascade refrigeration cycle. Energy Convers Manage 2015;105:509-517.
[31] Lawrence N, Elbel S. Theoretical and practical comparison of two-phase ejector refrigeration cycles including first and second Law analysis. Int J Refrig 2013;36(4):1220–1232.
[32] Zhao HX, Zhang K, Wang L, Han JT. Thermodynamic investigation of a booster-assisted ejector refrigeration system. Appl Therm Eng 2016;104:274-281.
[33] Trela M, Kwidzinski R, Butrymowicz D, Karwacki J. Exergy analysis of two-phase steam-water injector. Appl Therm Eng 2010;30:340-346.
[34] Fenton JD. On the energy and momentum principles in hydraulics. In: Proc. 31st Congress IAHR, 11–16 September 2005, Seoul. p. 625–636.
[35] Titus P, Damian T. Introduction to Fluid Mechanics, Fourth Edition. Wiley, New York: 1994.
[36] Bell IH, Wronski J, Quoilin S, Lemort V. Pure and pseudo-pure Fluid thermophysical property evaluation and the open-source thermophysical property library CoolProp. Ind Eng Chem Res 2014; 53(6):2498-2508.